ADVANCED PHOTONICS RESEARCH
Open Access
www.adpr-journal.com

Dispersion Analysis of Silver Thiogallate in a Broad Mid-Infrared Range

*Evgeniy S. Zatsepin, Artem S. Sabanin, Dmitriy V. Badikov, Sergei P. Kulik, and Anna V. Paterova**

Nonlinear optical materials designed for mid-infrared applications gain increasing interest in photonics and quantum-optical research. However, many of these materials remain unexplored in the broad mid-infrared range due to the limited availability of suitable equipment. Silver thiogallate ($AgGaS_2$) is one of the widely known nonlinear crystals used in mid-infrared frequency-conversion applications. While its transmission and refractive indices are well characterized up to 10.6 μm, dispersion properties beyond this wavelength remain unreported. In this work, a quantum-optical approach is employed to determine the refractive indices of $AgGaS_2$ across an extended mid-infrared wavelength range. Correlated photon pairs are generated in the crystal, where one photon in a pair is generated at a near-infrared wavelength and the other in the mid-infrared. Due to the correlations, detecting the spectrum of the near-infrared photons allows inferring the crystal's dispersion properties in the mid-infrared region up to 21 μm, without the need for infrared light sources or detectors. Sellmeier equations are further proposed that accurately describe both ordinary and extraordinary refractive indices across the entire transparency range of the crystal. The results are consistent with previously reported data below 10 μm and demonstrate the suitability of $AgGaS_2$ for frequency-conversion processes over an extended wavelength range.

1. Introduction

Nonlinear materials play a crucial role in nonlinear and quantum optics, particularly in frequency mixing processes such as sum- and difference-frequency generation, as well as up- and down-conversion. One promising research direction involves the use of nonlinear media for applications in the mid-infrared (mid-IR) spectral range. In this case, the requirements for nonlinear media include a broad transparency window at mid-IR range, robustness to high peak powers of the pump lasers, and high nonlinear conversion efficiency. One of such candidates is silver gallium sulfide ($AgGaS_2$ or AGS) nonlinear crystal also known as silver thiogallate. This crystal exhibits a broad transparency window, high nonlinearity among existing nonlinear materials, and a high damage threshold.[1,2] These properties enable its effective use in difference-frequency generation (DFG),[3] optical parametric oscillators,[4,5] optical parametric amplification[6,7] and optical parametric generation[8–11] in the mid-IR range. Moreover, AGS has been demonstrated in mid-IR metrology schemes based on nonlinear interferometry.[12–14] These applications highlight the importance of accurate dispersion analysis in AGS in the mid-IR range.

The dispersion characteristic of nonlinear crystals in the mid-IR range can be measured by classical methods, such as "minimum-deviation technique".[15,16] This method employs a tunable narrowband light beam, generated by an IR light source and a monochromator, which is then directed into a prism

E. S. Zatsepin, A. S. Sabanin, S. P. Kulik, A. V. Paterova
Laboratory of Quantum Engineering of Light
South Ural State University
Chelyabinsk 454080, Russia
E-mail: paterovaav@susu.ru

D. V. Badikov
High Technologies Laboratory
Kuban State University
Krasnodar 350040, Russia

The ORCID identification number(s) for the author(s) of this article can be found under https://doi.org/10.1002/adpr.202500267.

DOI: 10.1002/adpr.202500267

S. P. Kulik
Quantum Technology Centre
Faculty of Physics
Lomonosov Moscow State University
Moscow 119991, Russia

A. V. Paterova
Institute of Materials Research and Engineering
Agency for Science
Technology and Research
Singapore 138634, Republic of Singapore

fabricated from the material under study. Another classical approach involves harmonic generation (second harmonic generation or sum frequency generation) within the nonlinear crystal using IR laser sources.[17,18] However, the use of tunable IR light sources in these methods limits the range of wavelengths achievable at the experiments. Additionally, these techniques rely on direct detection using IR detectors, which often have low efficiency and may require cryogenic cooling.[15]

Another method for measuring the dispersion characteristics of nonlinear crystals is DFG.[3] This technique uses two single-mode diode lasers operating in the visible range to generate a mid-IR beam within the nonlinear crystal under study. Wavelength tunability is achieved by voltage ramping of the diode lasers. However, this limits the achievable single-mode operation range and consequently restricts the DFG tuning range. Additionally, the technique still relies on direct detection of the IR light. To overcome the limitations of IR detection, upconversion techniques can be employed, where an IR laser source is mixed with a visible laser in a nonlinear crystal to generate a beam in the visible range, facilitating easier detection.[19,20] However, this approach still requires a tunable IR source to cover a broad wavelength range, and involves the use of two lasers.

An alternative method for spectroscopy of nonlinear media in mid-IR range is using the quantum-optical phenomenon of spontaneous parametric down conversion (SPDC),[21] where photons from a laser pump source may spontaneously decay into a pair of correlated photons called signal (with higher energy) and idler. Depending on phase-matching requirements in the crystal the signal and idler SPDC photons can be generated having visible (or near-IR) and mid-IR wavelengths, respectively. Due to correlations between photons, the properties of the crystal in the IR range can be inferred by detecting the signal SPDC photons in the visible (or near-IR) spectrum. As a result, this technique does not require IR light sources or IR detection. The method has already been demonstrated using doped lithium niobate nonlinear crystals[22] and can be extended to other nonlinear materials.

The dispersion characteristics of AGS nonlinear crystals are known up to 10.6 μm,[18] but remain unreported beyond this range. In this work, we employ the SPDC generation technique to measure the refractive indices of AGS nonlinear crystals across a broad mid-IR wavelength range. Using a continuous-wave laser, we generate signal and idler SPDC photons in the near-IR and mid-IR regions, respectively. By detecting the spectrum of near-IR photons using a Si-based camera, we retrieve the dispersion characteristics of the AGS crystals up to 21 μm. Furthermore, we propose corrected Sellmeier equations to accurately describe the ordinary and extraordinary refractive indices of AGS crystal across a broad range of wavelengths. The obtained results are in good agreement with previously reported refractive index data up to 10 μm and enable precise modeling of nonlinear frequency-conversion processes in AGS over a broader spectral region that has not been previously explored.

2. Theory

The process of SPDC takes place in a nonlinear crystal, where the photons of the pump laser have a probability of decaying into a pair of correlated photons.[23] In the approximation of a collinear pump beam, and assuming that the transverse size of the laser mode is much smaller than the transverse dimensions of the crystal, the state vector of the biphoton field in Dirac notation is given by the following[24]

$$|\psi\rangle = |\mathrm{vac}\rangle + \sum_{k_p,\sigma_p}\sum_{k_s,\sigma_s}\sum_{k_i,\sigma_i} F(k_s,k_i)a^+_{k_s}a^+_{k_i}|\mathrm{vac}\rangle \tag{1}$$

where $|\mathrm{vac}\rangle$ is the initial vacuum state, $a^+_{k_s}$ and $a^+_{k_i}$ are creation operators of signal and idler photons in modes k_s and k_i, respectively, k_j ($j = p, s, i$) are respective wave vectors for pump, signal and idler photons, σ_j are the polarization states of the photons, $F(k_s, k_i)$ is the amplitude of the two-photon field, which is defined by the phase mismatch Δk in a nonlinear media[25]

$$F(k_s,k_i) \propto \mathrm{sinc}\left[\Delta k(k_s,k_i)\frac{L}{2}\right] \tag{2}$$

$$\Delta k(k_s,k_i) = |\vec{k}_p| - |\vec{k}_s| - |\vec{k}_i| = k_p - k_s\cos\theta_s - k_i\cos\theta_i \tag{3}$$

where L is the length of the nonlinear crystal, θ_s and θ_i are the emission angles of the signal and idler SPDC photons, respectively. The frequency-angular spectrum of signal SPDC is given by the square of the two-photon amplitude defined in Equation (2).

To obtain both ordinary (n^o) and extraordinary (n^e) refractive indices of the nonlinear crystal via SPDC generation method, one needs to exploit type II phase-matching requirements, where the extraordinary pump is converted into ordinary (signal) and extraordinary (idler) waves. In this case, taking into account energy conservation and the phase-matching conditions in the crystal, Equation (3) can be expressed as

$$\Delta k(\theta_c,\omega_s,\theta_s) = \frac{n_p(\theta_c)\omega_p}{c} - \frac{n_s\omega_s}{c}\sqrt{1-\left(\frac{\sin\theta_s}{n_s}\right)^2} - \frac{n_i(\theta_c)\cdot(\omega_p-\omega_s)}{c}\sqrt{1-\left(\frac{\omega_s\sin\theta_s}{n_i(\theta_c)\cdot(\omega_p-\omega_s)}\right)^2} \tag{4}$$

where θ_c is the phase matching angle defining the crystal cut, ω_s and ω_p are frequencies of the pump and signal photons, θ_s is the external emission angle of the signal SPDC photons outside of the nonlinear crystal, $n_p(\theta_c) = n_p^{\mathrm{eff}}(\theta_c, \omega_p)$, $n_s = n_s^o(\omega_s)$, $n_i(\theta_c) = n_i^{\mathrm{eff}}(\theta_c, \omega_p - \omega_s)$ are the refractive indices of the crystal at the frequencies of the pump, signal and idler photons, respectively. The effective refractive index $n_{p,i}^{\mathrm{eff}}$ for the extraordinary wave (for pump and idler waves) depends on the orientation of the nonlinear crystal θ_c and is given by[26]

$$n_{p,i}^{\mathrm{eff}}(\theta_c,n^o,n^e) = n_{p,i}^o\sqrt{\frac{1+\tan^2\theta_c}{1+\left(\frac{n_{p,i}^o}{n_{p,i}^e}\right)^2\tan^2\theta_c}} \tag{5}$$

Therefore, determining the ordinary and extraordinary refractive indices of the nonlinear crystal at the idler photon frequencies $n_i^{o,e}$ requires the acquisition of at least two signal SPDC

spectra at distinct phase-matching angles θ_{ca} in order to solve the corresponding system of equations

$$\Delta k(\theta_{ca}, \omega_s, \theta_s) = 0 \tag{6}$$

where Δk is given by Equation (4), and a denotes the equation number in the system.

3. Experimental setup

The experimental setup is shown schematically in **Figure 1**. In the experiment we use the near-IR continuous wave (cw) laser source (with 783.80 ± 0.02 nm wavelength, 120 mW power) to pump a silver thiogallate nonlinear crystal (with $L = 2$ mm length) characterized by a broad transparency range in the mid-IR (see Figure S1, Supporting Information). The crystal is cut for type II phase matching ($e \rightarrow o + e$) at an orientation of 51.1°, enabling the generation of SPDC photon pairs in a non-degenerate regime at room temperature. In this regime, the signal photons are produced in the near-IR wavelength range, while the idler photons are generated in the mid-IR region. The AGS crystal is integrated into a nonlinear interferometer setup consisting of a parabolic and a flat mirror (see Ref. [12] for more details). In this configuration, SPDC photon pairs are generated twice – once during the forward propagation of the pump beam and again upon its reflection. The detected interference in this case is given by the product of the spectrum of signal SPDC photons and the modulation component

$$I_s \sim \mathrm{sinc}^2(\Delta k L/2)[1 + \cos(\Delta k L + \Delta k' \varepsilon)] \tag{7}$$

where $\varepsilon/2$ is the displacement of the crystal from the focal distance f_1 of the parabolic mirror (PM), $\Delta k'$ is the phase mismatch in the medium outside of the crystal. The interference for the signal SPDC photons is recorded using a spectrometer and an electron-multiplying charge-coupled device (EMCCD) camera.

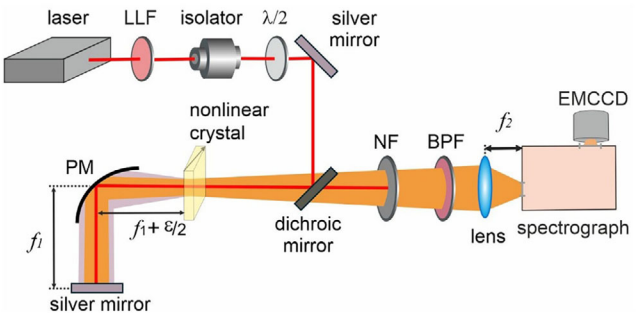

Figure 1. Experimental setup for measuring the spectrum of signal SPDC photons. The setup is based on a nonlinear interferometry scheme incorporating a nonlinear crystal, a PM, and a flat mirror. A cw laser is directed into the nonlinear crystal via a dichroic mirror, after passing through a laser line filter, an optical isolator, and a half-wave plate (λ/2). The generated signal SPDC photons are separated by the dichroic mirror, then pass through a pump-wavelength notch filter and a band-pass filter. The signal is subsequently focused by a lens system into the entrance slit of the spectrometer. The wavelength-angular spectrum of the signal SPDC photons is then recorded by an EMCCD camera positioned at the output of the spectrometer.

Incorporating a spectral instrument (spectrometer) to the recording system allows obtaining visual 2D spectra in wavelength-angle coordinates.

Spherical aberrations occurring at nonzero angles in the spectrometer are accounted for in the experiments, (see Figure S2, Supporting Information). The signal is detected in the near-IR wavelength range ≈815–880 nm, corresponding to the mid-IR range for the conjugate idler photons ≈7–21 μm. The refractive indices of the ordinary and extraordinary waves in the AGS crystal are determined by recording three SPDC spectra to enhance measurement accuracy and by solving a system of three equations $\Delta k(\theta_{ca}, n_o, n_e) = 0$.

The nonlinear interferometry scheme is not essential for characterization of the crystal, as a signal SPDC generation would suffice. However, registering the interference pattern of SPDC photons enables precise alignment of the lens system, the spectrometer, and the EMCCD camera to accurately capture the spectra of the signal SPDC photons in the wavelength-angular domain. Misalignment of the lenses or improper positioning of the camera can distort the spectra along the angular axis. The use of the interferometry scheme ensures that the system is aligned to record the spectra precisely at the Fourier plane, as any misalignment would result in blurred interference fringes. This scheme enables for the unambiguous transformation of angular coordinates into spatial ones, thereby significantly simplifying spectral processing.

4. Results

4.1. Observation of the Signal SPDC Spectra

During the experiments, the phase-matching angle of the AGS crystal is set to three different values and the crystal position to $\varepsilon_{exp} > 0$. The corresponding SPDC spectra are recorded within 20 s acquisition time and G = 295 multiplication parameter, see **Figure 2**. The spectra shown in Figure 2a–c are obtained using two sequential exposures on the EMCCD camera, as the system's spectral window is limited to ≈39.4 nm at the near-IR range, (see Figure S3, Supporting Information). The detected wavelengths of the signal SPDC photons range from 810.6 nm to 880 nm, corresponding to mid-IR idler wavelengths of ≈23.7 to 7.2 μm. The nonlinear interferometry scheme still enables measurement of the SPDC spectra. Only a portion of the spectrum is modulated due to the interference, which does not affect the main objectives of the experiments.

The recorded SPDC spectra exhibit a characteristic elliptical shape, consistent with previous studies reporting SPDC spectra extending into regions influenced by polariton scattering.[27,28] However, in the range of 825–832 nm, which corresponds to ≈13.8–15.7 μm in the mid-IR, the spectra broaden, see the detailed view in Figure 2d.

This range coincides with the two-phonon absorption bands of the AGS crystal.[29] Beyond 16 μm, the absorption decreases exhibiting a narrow transparency window up to 17.5 μm (see Figure S1, Supporting Information), while the SPDC spectra are observed up to 21 μm.[30,31] The spectral broadening within the ≈14–16 μm range can be attributed to light scattering by

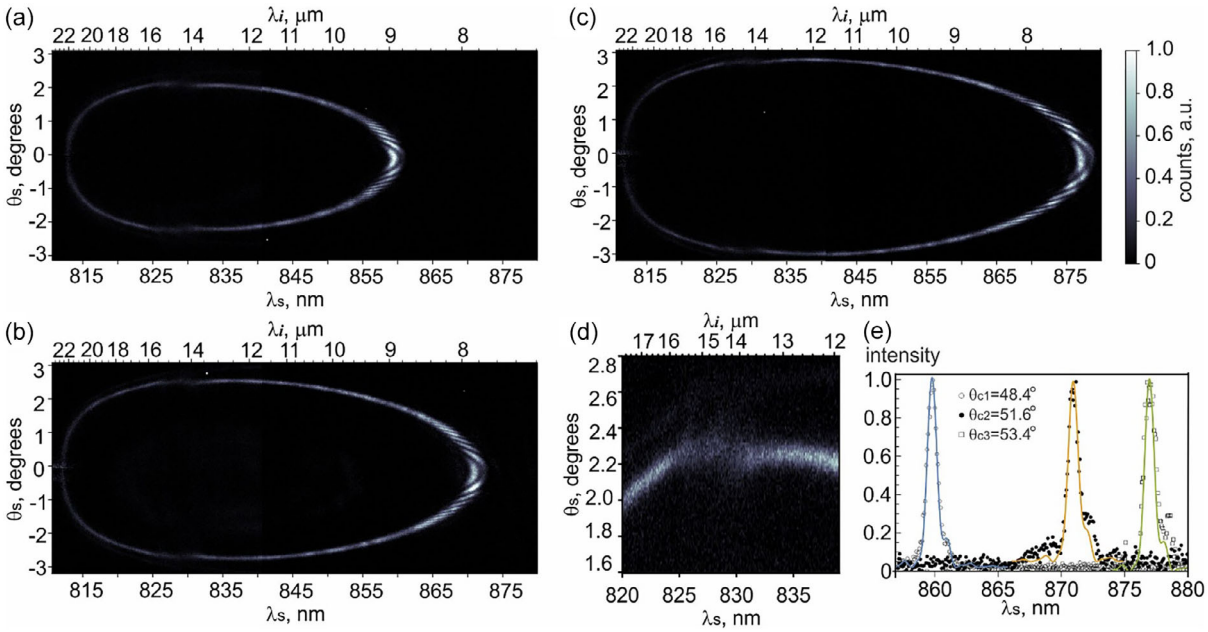

Figure 2. Wavelength-angular spectra of signal SPDC photons for the orientation of the nonlinear crystal θ_c at a) 48.4°, b) 51.6°, and c) 53.4°, respectively. The scale bar shown at (c) is applicable for graphs (a) and (b) as well. The detected wavelengths for signal SPDC photons are shown in lower *x*-axis and corresponding idler photon wavelengths – in upper *x*-axis. d) The part of the SPDC spectrum from graph (a) showing the region, where AGS crystal presents significant absorption. e) The spectra for signal SPDC photons at collinear angles $\theta_s = 0°$. The points correspond to experimentally measured spectra, and the solid curves show the corresponding theoretical plots.

polaritons, where the spectral profile is given by Lorentzian line shape.[28,32–34]

The experimental phase-matching angles set for the AGS crystal can be determined from Figure 2a–c, since in all three spectra the idler SPDC photon wavelengths in the collinear regime are below 10.6 μm, where the refractive indices of the crystal are known.[17,18] The corresponding collinear SPDC spectra for the signal photons are presented in Figure 2e. The phase-matching angles obtained from the experimental measurements are $48.40° \pm 0.04°$, $51.60° \pm 0.04°$, and $53.40° \pm 0.04°$, respectively. Theoretical SPDC spectra, accounting for the interference modulation observed within the spectra, are shown by the solid curves in Figure 2e.

4.2. Analysis of the SPDC Spectra

To further analyze the spectra of signal SPDC photons, we apply a blurring filter to the experimental data to reduce interference modulation effects, (see Figure S3, Supporting Information). Using these processed spectra and the known phase-matching angles θ_{ca} $(a = 1,2,3)$, we solve the system of three nonlinear equations (6), (see Figure S4, Supporting Information), to obtain the wavelength-dependent effective refractive indices for idler photons $n_i^{\text{eff}}(\theta_{ca}, n_i^o, n_i^e)$, where the idler wavelength λ_i is given by $\lambda_i = \frac{\lambda_s \lambda_p}{\lambda_s - \lambda_p}$. Next, taking into account the ellipsoid of the refractive indices from Equation (5), we determine the ordinary n_i^o and extraordinary n_i^e refractive indices of the crystal by numerically minimizing the corresponding system of equations using the nonlinear least-squares method

$$\frac{1}{[n_i^{\text{eff}}(\theta_{ca})]^2} - \frac{\cos^2\theta_{ca}}{[n_i^o]^2} - \frac{\sin^2\theta_{ca}}{[n_i^e]^2} \to 0 \tag{8}$$

The results for ordinary n_i^o and extraordinary n_i^e refractive indices of the AGS crystal at the mid-IR range are presented in **Figure 3**a.

Both refractive index curves exhibit distinct reoscillations around 15 μm, indicating the presence of absorption bands of the crystal in this region.[29,30] The accuracy of refractive index estimation in our measurements is on the order of 10^{-3}, which is sufficient for a wide range of mid-IR optical applications. This is also proven with measurement of the experimental SPDC spectra for the phase-matching angle $\theta_c = 43.03 \pm 0.04°$, where wavelengths for the idler SPDC photons are greater 10.6 μm, see Figure 3b.

In Figure 3b the upper half of the graph shows the theoretical spectrum calculated using refractive indices from Figure 3a, and the lower half corresponds to the measured spectrum. (The whole data is shown in Figure S5, Supporting Information.) The experimental and theoretical spectra in Figure 3b are in good agreement, confirming that the derived refractive indices are suitable for determining the phase-matching conditions in nonlinear frequency conversion processes.

Figure 3a also shows a comparison of the obtained data with the Sellmeier equations for AGS crystal from Ref. [18] We note that the curves for the refractive indices from literature in Figure 3a agrees with the obtained data up to ≈13.7 μm for extraordinary waves and up to ≈14.7 μm for ordinary waves. For longer wavelengths the corrected Sellmeier coefficients are needed. Therefore, we approximate the measured refractive indices with the new Sellmeier equations, see **Figure 4**.

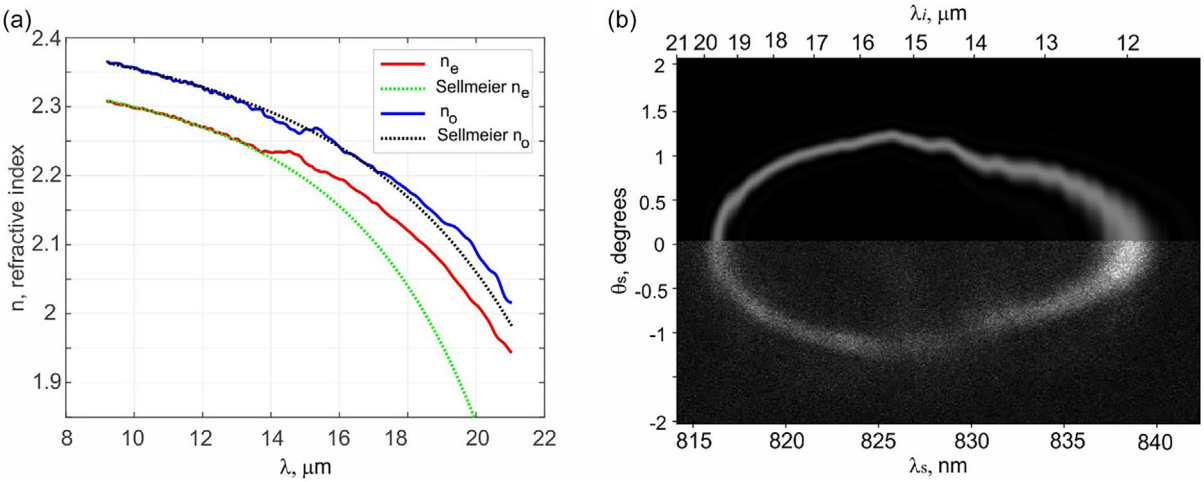

Figure 3. a) Calculated refractive indices of AGS crystal for ordinary and extraordinary waves. Solid curves correspond to calculated refractive indices, dotted curves show refractive indices from Ref. [18] b) Spectrum for signal SPDC photos from AGS crystal oriented at $\theta_c = 43.03 \pm 0.04°$. The detected wavelengths for signal SPDC photons are shown in lower *x*-axis and corresponding idler photon wavelengths - in upper *x*-axis.

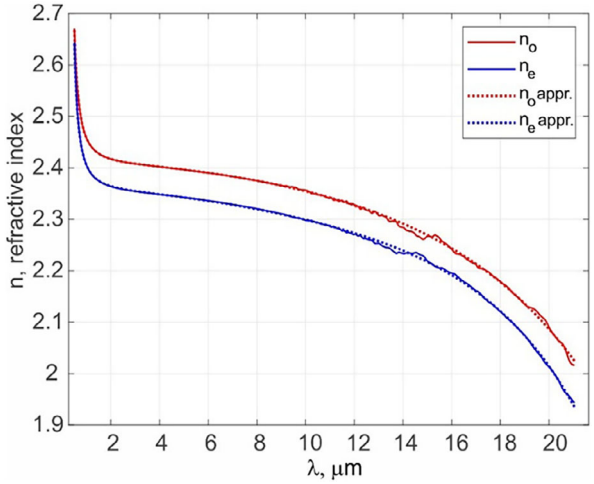

Figure 4. Refractive indices fitted with Sellmeier equations. Solid curves before 10.6 μm correspond to Sellmeier equations from Ref. [18] Solid curves beyond 10.6 μm show calculated ordinary and extraordinary refractive indices in our measurements. Dotted curves show the approximations with new Sellmeier coefficients given in Equation (9 and 10).

$$n_e^2 = 5.5465 + \frac{0.2163}{\lambda^2 - 0.101} - 2.7694 \cdot 10^{-3}\lambda^2 + 2.5684 \cdot 10^{-6}\lambda^4 - 1.2795 \cdot 10^{-8}\lambda^6 \quad (9)$$

$$n_o^2 = 5.7929 + \frac{0.2301}{\lambda^2 - 0.078} - 2.3138 \cdot 10^{-3}\lambda^2 - 1.4579 \cdot 10^{-6}\lambda^4 - 0.4032 \cdot 10^{-8}\lambda^6 \quad (10)$$

The new Sellmeier coefficients accurately describe the refractive indices over a wide spectral range from the visible region up to 21 μm (with the exception of the regions with scattering on polaritons, that are not included in the approximation). The theoretical SPDC spectrum for the AGS crystal, calculated using Equation (9 and 10), agrees well with the experimental results as well, (see Figure S6, Supporting Information).

5. Discussion and Conclusion

AGS is a chalcopyrite crystal with a tetragonal structure in $\bar{4}2\,m$ space group.[35] Growing high-quality AGS crystals is a challenging task due to its congruent melting and tendency to form defects. The most common and effective method for growing AGS crystals is the Bridgman-Stockbarger method. It involves slowly moving an ampoule with molten material through a temperature gradient, which leads to crystallization. Precise control of both the growth rate and the temperature gradient is crucial for producing high-quality crystals. Following growth, the crystal undergoes additional annealing to remove scattering centers. Strict adherence to all technological procedures enables the fabrication of high-quality AGS crystals with absorption coefficients below 0.005 cm^{-1}, as used in our experiments. Generally, AGS crystal is known to be transparent up to 13 μm. However, there is a narrow transmission window of AGS crystal after a strong absorption band at 13.8–15.7 μm,[31,36] as also demonstrated in our work (see Figure S1, Supporting Information).

The lattice parameters, refractive indices, and other properties of AGS can vary slightly depending on the growth methods and technologies used.[37] However, variations introduced by different growth techniques do not result in significant changes in the crystal's linear or nonlinear-optical properties.[38,39] Therefore, the reported Sellmeier coefficients in Equation (9 and 10) should be accurate for the AGS crystals grown using different methods.

Equation (9 and 10) describe the refractive indices of AGS crystals up to 21 μm, as no phase matching is observed for SPDC generation at longer wavelengths. This limitation is primarily due to the strong absorption of AGS in this spectral region. However, beyond 100 cm^{-1} ($\lambda > 100$ μm), the absorption decreases again,[40] suggesting potential applications and

characterization of the crystal in the THz range using the demonstrated method. Moreover, the presented refractive index calculation method is not limited to AGS crystal. It can be extended to other nonlinear crystals. Recent studies highlight several promising materials for mid-IR nonlinear optics,[41,42] further expanding the applicability of this approach.

In conclusion, in this work we demonstrated the use of SPDC for measuring the refractive indices of a nonlinear crystal across a broad mid-IR wavelength range. Operating in a non-degenerate SPDC regime enables indirect characterization the mid-IR optical properties of crystals by detecting correlated near-IR photons with conventional Si-based detectors and available optics. Using this approach, we determined the refractive indices of an AGS nonlinear crystal up to 21 μm, while performing detection in the 815-880 nm range. It should be noted that the approach used in the work allowed us to advance into the long-wave region despite the strong lattice absorption of the crystal, which is hardly possible using classical methods. Whereas previous studies reported AGS refractive indices only up to 10.6 μm, our results extend the Sellmeier equations to longer mid-IR wavelengths. The achieved accuracy of the method is on the order of $1{\cdot}10^{-3}$, making it suitable for precise dispersion characterization of nonlinear crystals in mid-IR range.

Although AGS is often reported in the literature to be transparent only up to 13 μm, in practice it exhibits a narrow transparency window around ≈15.7–17.5 μm,[36,43] allowing for the nonlinear conversion up to 21 μm in our experiments. This advancement highlights the importance of investigation of the nonlinear crystal in extended range of IR wavelengths to broaden their usage in frequency-conversion possesses, including SPDC processes in nonlinear interferometry schemes.[12–14]

Supporting Information

Supporting Information is available from the Wiley Online Library or from the author.

Acknowledgements

This work was supported by the Government of the Russian Federation (Grant No. 075-15-2025-018, dated February 27, 2025) and by South Ural State University, where part of the experimental data was collected and analytical simulations were conducted. A.P. additionally acknowledges support from the Agency for Science, Technology and Research (A*STAR), which facilitated the acquisition of the experimental data. A.S. and A.P. are grateful to Viktor Khristenko's grant program "Step into the Future" for supporting the theoretical simulations of the work. E.Z., S.K., and A.P. acknowledge support from the State Assignment FENU-2024-0002, which enabled the detailed analysis and interpretation of the experimental results.

Conflict of Interest

The authors declare no conflict of interest.

Data Availability Statement

The data that support the findings of this study are available from the corresponding author upon reasonable request.

Keywords

nonlinear materials, nonlinear optics, quantum optics

Received: September 17, 2025
Revised: November 1, 2025
Published online:

[1] V. Petrov, *Opt. Mater.* **2012**, *34*, 536.
[2] A. Harasaki, K. Kato, *Jap. J. Appl. Phys.* **1997**, *36*, 700.
[3] U. Willer, T. Blanke, Wolfgang Schade, *Appl. Opt.* **2001**, *40*, 5439.
[4] K. L. Vodopyanov, J. P. Maffetone, I. Zwieback, W. Ruderman, *Appl. Phys. Lett.* **1999**, *75*, 1204.
[5] N. Hendaoui, A. Peremans, P. G. Schunemann, K. T. Zawilski, V. Petrov, *Laser Phys.* **2013**, *23*, 085401.
[6] A. Pushkin, E. Migal, D. Suleimanova, E. Mareev, F. Potemkin, *Photonics* **2022**, *9*, 90.
[7] E. A. Migal, F. V. Potemkin, V. M. Gordienko, *Opt. Lett.* **2017**, *42*, 5218.
[8] S. A. Andreev, N. P. Andreeva, M. S. Barashkov, V. V. Badikov, V. K. Demkin, A. K. Don, V. M. Epikhin, M. I. Krymskii, Yu. K. Kalinnikov, K. V. Mitin, A. M. Seregin, V. V. Sinaiskii, M. A. Talalaev, A. A. Chistyakov, N. I. Shchebetova, T. A. Shchetinkina, *Quantum Electron.* **2010**, *40*, 288.
[9] V. V. Badikov, P. S. Blinov, A. A. Kosterev, V. S. Letokhov, A. L. Malinovsky, E. A. Ryabov, *Quantum Electron.* **1997**, *27*, 523.
[10] E. S. Voronin, V. S. Solomatin, N. I. Cherepov, V. V. Shuvalov, V. V. Badikov, O. N. Pivovarov, *Sov. J. Quantum Electron.* **1975**, *5*, 97.
[11] S. A. Andreev, I. N. Matveev, I. P. Nekrasov, S. M. Pshenichnikov, N. P. Sopina, *Sov. J. Quantum Electron.* **1977**, *7*, 366.
[12] A. V. Paterova, Z. S. D. Toa, H. Yang, L. A. Krivitsky, *ACS Photon.* **2022**, *9*, 2151.
[13] Y. Mukai, R. Okamoto, S. Takeuchi, *Opt. Express* **2022**, *30*, 22624.
[14] A. Sabanin, A. Paterova, *Laser Phys. Lett.* **2025**, *22*, 015205.
[15] W. L. Bond, *J. Appl. Phys.* **1965**, *36*, 1674.
[16] G. Boyd, H. Kasper, J. McFee, *IEEE J. Quantum Electron.* **1971**, *7*, 563.
[17] E. Tanaka, K. Kato, *Appl. Opt.* **1998**, *37*, 561.
[18] K. Kato, T. Okamoto, S. Grechin, N. Umemura, *Crystals* **2019**, *9*, 129.
[19] D. A. Kleinman, G. D. Boyd, *J. Appl. Phys.* **1969**, *40*, 546.
[20] G. C. Bhar, S. Das, U. Chatterjee, R. S. Feigelson, R. K. Route, *Appl. Phys. Lett.* **1989**, *54*, 1489.
[21] D. N. Klyshko, *Photons and Nonlinear Optics*, Gordon & Breach Science, New York **1988**.
[22] A. L. Aleksandrovskii, G. I. Ershova, G. K. Kitaeva, S. P. Kulik, I. I. Naumova, V. V. Tarasenko, *Sov. J. Quantum Electron.* **1991**, *21*, 225.
[23] D. N. Klyshko, *Soviet Phys. JETP* **1969**, *28*, 522.
[24] M. H. Rubin, D. N. Klyshko, Y. H. Shih, A. V. Sergienko, *Phys. Rev. A* **1994**, *50*, 5122.
[25] L. J. Wang, X. Y. Zou, L. Mandel, *Phys. Rev. A* **1991**, *44*, 4614.
[26] V. G. Dmitriev, G. G. Gurzadyan, D. N. Nikogosyan, *Handbook of Nonlinear Optical Crystals*, 3rd edition Springer, Berlin **1991-1999**.
[27] D. N. Klyshko, A. N. Penin, B. F. Polovnikov, *ZhETF Pis. Red.* **1970**, *11*, 11.
[28] Y. N. Polivanov, *Sov. Phys. Usp.* **1978**, *21*, 805.
[29] G. C. Bhar, R. C. Smith, *IEEE J. Quantum Electron.* **1974**, *10*, 546.
[30] G. C. Bhar, R. C. Smith, *Phys. Stat. Sol.* **1972**, *13*, 157.
[31] R. J. Seymour, F. Zernike, *Appl. Phys. Lett.* **1976**, *29* ,705.
[32] D. N. Klyshko, *Zh. Eksp. Teor. Fiz.* **1968**, *55*, 1006.
[33] A. V. Burlakov, Y. B. Mamaeva, A. N. Penin, M. V. Chekhova, *J. Exp. Theor. Phys.* **2001**, *93*, 55.

[34] G. K. Kitaeva, A. A. Mikhailovsky, P. S. Losevsky, A. N. Penin, *Opt. Commun.* **1997**, *138*, 242.
[35] S. C. Abrahams, J. L. Bernstein, *J. Chem. Phys.* **1973**, *59*, 1625.
[36] D. S. Chemla, P. J. Kupecek, D. S. Robertson, R. C. Smith, *Opt. Commun.* **1971**, *3*, 29.
[37] D. N. Nikogosyan, *Nonlinear Optical Crystals: A Complete Survey*, Springer-Science, New York **2005**.
[38] B. Chen, S. Zhu, B. Zhao, J. Zhang, Y. Huang, M. Li, J. Liu, B. Tan, R. Wang, Z. He, *J. of Crystal Growth* **2006**, *292*, 490.
[39] G. C. Catella, D. Burlage, *MRS Bull.* **1998**, *23*, 28.
[40] G. D. Holah, *Opt. Commun.* **1972**, *5*, 10.
[41] N. Kostyukova, E. Erushin, A. Boyko, G. Shevyrdyaeva, D. Badikov, *Photonics* **2024**, *11*, 281.
[42] V. V. Badikov, D. V. Badikov, V. B. Laptev, K. V. Mitin, G. S. Shevyrdyaeva, N. I. Shchebetova, V. Petrov, *Opt. Mater. Express* **2016**, *6*, 2933.
[43] I. O. Kinyaevskiy, A. V. Koribut, Y. V. Grudtsyn, M. V. Ionin, Y. M. Klimachev, N. N. Yudin, A. A. Ionin, *Opt. Laser Technol.* **2025**, *183*, 112270.